CHEMISTRY OF MATERIALS

Article

pubs.acs.org/cm

Electronic Structure Descriptor for the Discovery of Narrow-Band Red-Emitting Phosphors

Zhenbin Wang,[†] Iek-Heng Chu,[†] Fei Zhou,[‡] and Shyue Ping Ong*[,†]

[†]Department of NanoEngineering, University of California San Diego, 9500 Gilman Drive, La Jolla, California 92093-0448, United States

[‡]Physics Division, Lawrence Livermore National Laboratory, 7000 East Avenue, Livermore, California 94550, United States

Supporting Information

ABSTRACT: Narrow-band red-emitting phosphors are a critical component of phosphor-converted light-emitting diodes for highly efficient illumination-grade lighting. In this work, we report the discovery of a quantitative descriptor for narrow-band Eu^{2+}-activated emission identified through a comparison of the electronic structures of known narrow-band and broad-band phosphors. We find that a narrow emission bandwidth is characterized by a large splitting of more than 0.1 eV between the two highest Eu^{2+} $4f^7$ bands. By incorporating this descriptor in a high-throughput first-principles screening of 2259 nitride compounds, we identify five promising new nitride hosts for Eu^{2+}-activated red-emitting phosphors that are predicted to exhibit good chemical stability, thermal quenching resistance, and quantum efficiency, as well as narrow-band emission. Our findings provide important insights into the emission characteristics of rare-earth activators in phosphor hosts and a general strategy to the discovery of phosphors with a desired emission peak and bandwidth.

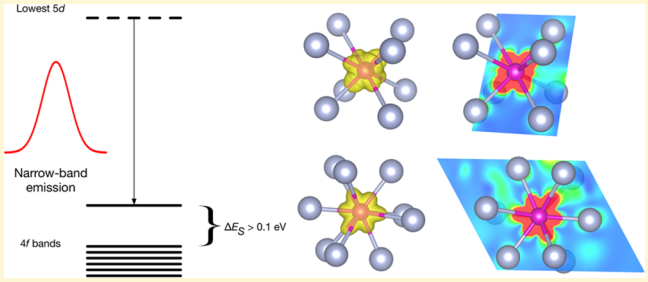

INTRODUCTION

Phosphor-converted light-emitting diodes (pc-LEDs) are an energy efficient and environmentally friendly lighting source for solid-state lighting.[1−7] For illumination-grade lighting, a warm white light LED with a high luminous efficacy and color rendering index is desirable. A common strategy to improve the color rendering index is to add a red-emitting component into an LED. In recent years, Eu^{2+}-activated nitride phosphors have emerged as highly promising red-emitting phosphors for pc-LEDs due to their high chemical and thermal stabilities, small thermal quenching, and high quantum efficiency (QE).[8−10] Unfortunately, the broad bandwidth and/or deep red maximum of the emission spectra of commercial red-emitting phosphors lead to a substantial portion of the emitted energy being outside the range of human vision, severely reducing the luminous efficacy of the LED. For example, although the widely used commercial $CaAlSiN_3$:Eu^{2+} phosphor has an excellent QE > 95% at 150 °C,[1] its emission peak (λ_{em} ~ 650 nm)[2] is too red-shifted and its bandwidth (characterized by the full width at half-maximum, or fwhm, ~90 nm) is too broad.

Recently, Pust et al.[5] reported the discovery of a highly promising narrow-band red-emitting phosphor, $SrLiAl_3N_4$:Eu^{2+}, with an emission peak position at ~650 nm and a fwhm of ~50 nm. A 14% improvement in luminous efficacy was achieved with $SrLiAl_3N_4$:Eu^{2+} as a red-emitting component in a pc-LED compared with that of a commercial LED device.[5] The luminous efficacy would be further enhanced if the emission maximum of $SrLiAl_3N_4$:Eu^{2+} could be blue-shifted, but the activator concentration is found to have little influence on the emission band position. The chemically similar $CaLiAl_3N_4$:Eu^{2+} narrow-band red-emitting phosphor also has an emission peak that is too deep red (λ_{em} ~ 668 nm) for high-powered LEDs.[6] Another narrow-band red-emitting phosphor, $SrMg_3SiN_4$:Eu^{2+}, has an ideal peak position at ~615 nm and a narrow bandwidth of ~43 nm.[7] However, the thermal quenching of $SrMg_3SiN_4$:Eu^{2+} is too severe for practical applications. Despite these discoveries, the overall number of known narrow-band red-emitting phosphors remains very small. The development of highly efficient narrow-band red-emitting phosphors with an optimal spectral peak position (λ_{em} ~ 615 nm) and a narrow width (fwhm <50 nm) is therefore a critical materials challenge for warm white illumination-grade lighting.[11,12]

In this work, we report the discovery of a quantitative descriptor for narrow-band Eu^{2+}-activated emission that emerged from a comparison of the first-principles electronic structures of nine well-known phosphors. We then identified five new narrow-band red-emitting phosphors, $CaLiAl_3N_4$ ($P\bar{1}$), $SrLiAl_3N_4$ ($I4_1/a$), $SrLiAl_3N_4$ ($P\bar{1}$), $SrMg_3SiN_4$ ($P\bar{1}$), and $BaLiAl_3N_4$ ($P\bar{1}$), for high-power pc-LED applications through a high-throughput screening of ternary and quaternary nitride compounds. These five new phosphors are predicted to satisfy a

Received: April 14, 2016
Revised: May 9, 2016
Published: May 9, 2016

DOI: 10.1021/acs.chemmater.6b01496
Chem. Mater. 2016, 28, 4024−4031

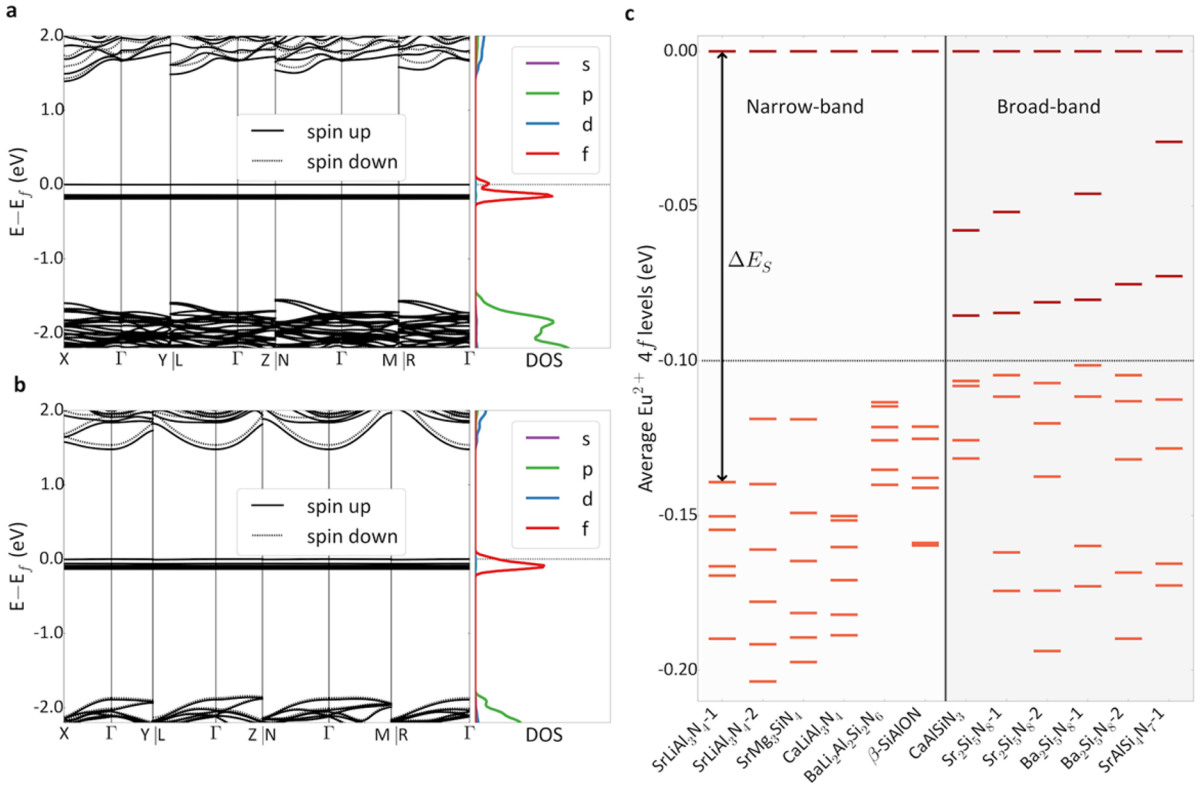

Figure 1. Electronic structures for selected (oxy)nitride phosphors. (a) Band structure and density of states (DOS; arbitrary units) of a narrow-band red-emitting phosphor, $SrLiAl_3N_4:Eu^{2+}$. (b) Band structure and DOS (arbitrary units) of a broad-band red-emitting phosphor, $CaAlSi_3N_4:Eu^{2+}$. (c) Average Eu^{2+} 4f band levels for five narrow-band and four broad-band phosphors. A numbered suffix (e.g., "-1") is added where necessary to distinguish between distinct Eu^{2+} activator sites in the same host structure, with increasing numbers indicating increasing site energy. The highest 4f band, which lies on the Fermi level, is set at 0 eV for ease of comparison.

balance of chemical stability, good thermal quenching behavior and quantum efficiency, and narrow-band emission.

METHODS

Structure Relaxation and Energy Calculations. Spin-polarized density functional theory calculations were performed using the Vienna *ab initio* simulation package (VASP) within the frozen-core projector-augmented wave method.[13,14] The generalized gradient approximation Perdew–Burke–Ernzerhof (PBE) functional[15] was used for all structural relaxations and energy calculations. A plane wave energy cutoff of 520 eV was used, and the electronic energy and atomic forces were converged to within 10^{-5} eV and 0.01 eV/Å, respectively. The Brillouin zone was integrated with a *k*-point density of 1000 per reciprocal atom. All crystal structure manipulations and data analysis were carried out using the Python Materials Genomics package.[16]

Energy above Hull, E_{hull}. The phase stability of predicted materials was estimated by calculating the energy above the linear combination of stable phases in the first-principles phase diagram,[17] also known as the energy above hull, E_{hull}. For phase diagram construction, the energies of all compounds other than those of direct interest in this work were obtained from the Materials Project[18] using the Materials Application Programming Interface.[18,19]

Host Band Gap E_g and Band Structure of Eu^{2+}-Activated Phosphors. The band gaps for all host materials were calculated using the PBE functional as well as the more accurate screened hybrid Heyd–Scuseria–Ernzerhof (HSE)[20,21] functional. To obtain the band structure and 4f levels of Eu^{2+}-activated phosphors, supercell models were constructed with relatively low Eu^{2+} doping concentrations (<10%) to mimic experimental doping levels. PBE calculations with a Hubbard *U*[22] parameter of 2.5 eV[23] for Eu was used for these relatively large systems. A Gaussian smearing of 0.05 eV was used for all band structure and density of states calculations. All electronic structure calculations of the Eu^{2+}-activated phosphors were performed without spin–orbital coupling (SOC) as the difficult convergence of SOC calculations makes them unsuitable for a high-throughput screening effort. Nevertheless, we performed SOC analyses on the new narrow-band red-emitting phosphors identified and confirmed that the relevant electronic structure feature, i.e., a large splitting in the top two 4f bands, does not change significantly with the inclusion of SOC.

Debye Temperature, Θ_D. The Debye temperature, Θ_D, was calculated using the quasi-harmonic model.[24] The elastic tensor was calculated with more stringent electronic convergence criterion of 10^{-6} eV per formula unit, and the elastic moduli were calculated using the Voigt–Reuss–Hill approximation.[25]

RESULTS

Descriptor for Narrow-Band Emission. The emission spectrum of Eu^{2+}-activated phosphors is attributed to the $4f^65d^1 \rightarrow 4f^7$ electronic transition. We therefore begin with a hypothesis that narrow- and broad-band emissions can be identified by differences in the electronic band structure. In this work, we adopt the definition of having a measured fwhm < 60 nm as a narrow-band emitter. The calculated electronic band structures of two representative red-emitting phosphors, $SrLiAl_3N_4:Eu^{2+}$ (narrow-band) and $CaAlSiN_3:Eu^{2+}$ (broad-band), are shown in Figure 1, panels a and b, respectively. We find that the Eu^{2+} 4f bands are very narrowly distributed in energy and that the energy level of each band may be estimated by averaging across all *k*-points.

Figure 1c shows the average Eu^{2+} 4f band levels of five narrow-band ($SrLiAl_3N_4:Eu^{2+}$, $SrMg_3SiN_4:Eu^{2+}$, $CaLiAl_3N_4:Eu^{2+}$, $BaLi_2Al_2Si_2N_6:Eu^{2+}$, and $Si_{141}Al_3ON_{191}$(*β*-SiAlON):Eu^{2+})[5−7,26,27] and four broad-band ($CaAlSiN_3:Eu^{2+}$,

DOI: 10.1021/acs.chemmater.6b01496
Chem. Mater. 2016, 28, 4024−4031

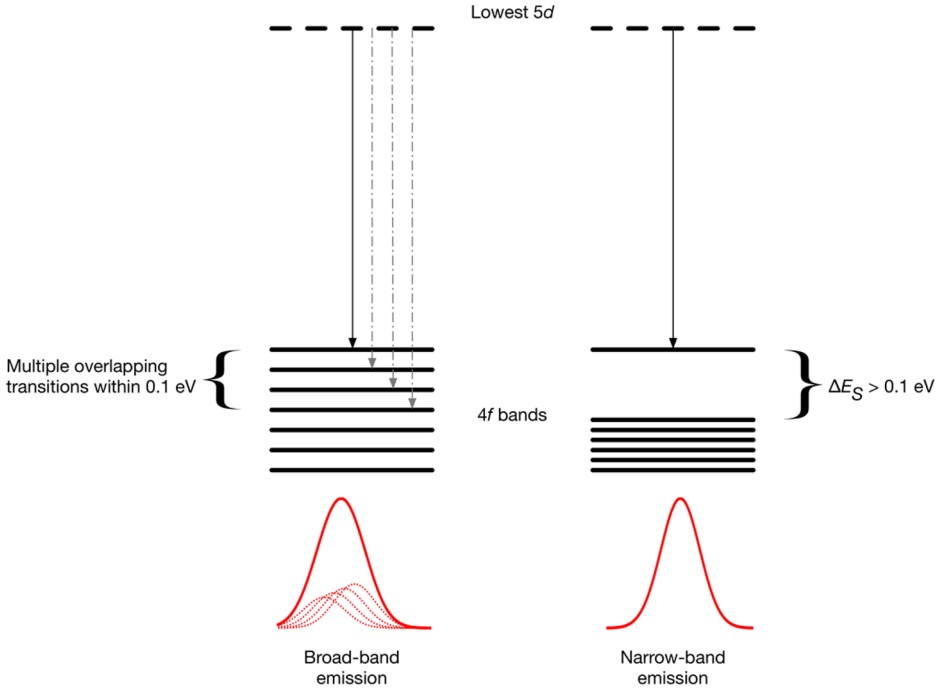

Figure 2. Relationship between emission bandwidth and Eu^{2+} 4f band levels. When there are multiple Eu^{2+} 4f levels within 0.1 eV from the highest band (left), overlapping emissions result in a broad bandwidth. Conversely, a large energy splitting, ΔE_S, of >0.1 eV between the two highest 4f bands (right) results in narrow-band emission.

Table 1. Calculated Properties of 10 Known Hosts for Red-Emitting Phosphors[a]

materials	space group	E_{hull} (meV)	E_g (eV) PBE	E_g (eV) HSE	E_g (eV) exp.	Θ_D (K)
$SrLiAl_3N_4$	$P\bar{1}$	0	2.97	4.47	4.56,[42] 4.70[5]	716
$SrMg_3SiN_4$	$I4_1/a$	0	2.42	3.68	3.90[7]	648
$CaLiAl_3N_4$	$I4_1/a$	13	3.03	4.45		743
$CaAlSiN_3$[b]	Cc	0	3.40	4.76	4.80,[3] 5.0−5.2[2]	787
$Ca_2Si_5N_8$	Cc	0	3.34	4.62	4.96,[28] 4.9[43]	788
$Sr_2Si_5N_8$	$Pmn2_1$	0	3.20	4.40	4.67,[28] 4.5[43]	709
$Ba_2Si_5N_8$[c]	$Pmn2_1$	0	2.88	4.06	4.59,[28] 4.1[43]	661
$SrAlSi_4N_7$	$Pna2_1$	31	3.58	4.72		745
$SrSiN_2$	$P2_1/c$	0	2.95	4.18	4.20[34]	375
$BaSiN_2$	$Cmca$	0	2.92	4.03	4.10[34]	360

[a]The band gap E_g was calculated using the PBE and screened hybrid HSE functionals. Experimental E_g values, where available, are presented for comparison. E_{hull} and Θ_D were calculated using the PBE functional. [b]$CaAlSiN_3$ has a disordered structure ($Cmc2_1$). Here, the lowest energy ordered structure (Cc) is presented. [c]Due to the wide variation in the experimentally reported E_g for $Ba_2Si_5N_8$, G_0W_0 calculations were performed for $Ba_2Si_5N_8$ and $BaSiN_2$. The calculated G_0W_0 band gaps for $Ba_2Si_5N_8$ and $BaSiN_2$ are 4.14 and 4.12 eV, respectively, in excellent agreement with the HSE results.

$Sr_2Si_5N_8:Eu^{2+}$, $Ba_2Si_5N_8:Eu^{2+}$, and $SrAlSi_4N_7:Eu^{2+}$)[2,28,29] phosphors derived from their calculated band structures (Figure S1). With the exception of green-emitting $BaLi_2Al_2Si_2N_6:Eu^{2+}$ and β-SiAlON:Eu^{2+}, all of the remaining phosphors exhibit red emission. Interestingly, we find that all narrow-band phosphors, regardless of their emission color, have a distinct large energy splitting, ΔE_S, of >0.1 eV between the two highest Eu^{2+} 4f bands. Broad-band emitters, on the other hand, have a more uniform 4f band distribution, with several bands lying within 0.1 eV of the highest 4f band at the Fermi level. It should be noted that we have tested the sensitivity of this analysis with respect to the U value for Eu (Figure S2) and found that the change in the difference in ΔE_S between narrow- and broad-band emitters is negligible for $1 < U < 5$ eV. We also find that the calculated ΔE_S shows an inverse relationship with respect to their experimentally measured fwhm, as shown in Figure S3.

We provide a justification for this distinct narrow-band electronic structure feature by considering the fact that broad-band emission is the result of multiple overlapping emission spectra occurring within the red spectra region. Multiple emission spectra can be the result of either multiple distinct activator sites with similar doping energies[1,28] or multiple transitions even within the same activator site. Figure 2 shows a schematic of the different transitions in broad- and narrow-band phosphors. In both cases, the main emission is the result of the transition of an electron from the lowest 5d band into the empty top 4f band, i.e., a $4f^6 5d^1 \rightarrow 4f^7$ transition. However, when there are other 4f bands within 0.1 eV of the top band, transitions to lower 4f bands may occur, resulting in

DOI: 10.1021/acs.chemmater.6b01496
Chem. Mater. 2016, 28, 4024−4031

overlapping emissions within ∼30 nm of the main peak and broadening of the emission. Therefore, we propose $\Delta E_S > 0.1$ eV as a threshold for narrow-band emission. We have tested the sensitivity of the screening results to the value of this threshold, as outlined in subsequent sections.

Parameterization of High-Throughput Screening Criteria. For commercial applications, a red-emitting phosphor host must satisfy a demanding set of properties, namely, good phase stability, emission in the red−orange region of the visible spectrum, excellent thermal quenching resistance, and high photoluminescence quantum efficiency. The phase stability of a material can be estimated by calculating the energy above the linear combination of stable phases in the phase diagram, also known as E_{hull}. Stable materials have an E_{hull} of 0 eV, and the more unstable a material, the higher E_{hull}. The emission wavelength has a direct relationship to the band gap E_g of the host material as the conduction band minimum of the host sets the energy level of the excited Eu^{2+}-activated phosphor (see Figure S4).[30] In general, host materials that are rigid and have large photoionization energy,[30] defined as the energy gap between the conduction band minimum of the host and the lowest 5d levels of the activator, exhibit higher quantum efficiencies, especially at elevated temperatures. The rigidity of a crystal can be estimated by its Θ_D[24] and the host band gap E_g may be used as a proxy to estimate the photoionization energy.

We parametrized the criteria for our high-throughput screening of nitrides through an analysis of the E_g and Θ_D of 10 well-known red-emitting phosphor hosts, summarized in Table 1. Unsurprisingly, the E_g calculated using the PBE[15] functional underestimates the experimental E_g by around 28−38% due to the well-known self-interaction error and lack of derivative discontinuity in semilocal exchange-correlation functionals.[31] The screened hybrid HSE[20,21] functional yields E_g that are in much better agreement (within 0.3 eV) with the experimental values.

The key observation from Table 1 is that despite the systematic underestimation of E_g by PBE the relative trends in E_g are generally well-reproduced, consistent with previous first-principles studies.[32] Hence, an efficient screening of E_g may be carried out using the computationally inexpensive PBE functional for a large number of compounds, followed by a more accurate secondary screening with the expensive HSE functional for a more limited subset of compounds. From Table 1, we find that the PBE and HSE E_g for red-emitting phosphors lie in the range of 2.42−3.58 and 3.68−4.76 eV, respectively. We also observe that the known phosphor nitrides have relatively high Θ_D of more than 500 K, with the exception of $SrSiN_2$ and $BaSiN_2$. Indeed, $SrSiN_2$ and $BaSiN_2$ have nonrigid layered crystal structures,[33] and the Eu^{2+}-activated hosts show relatively poor quantum efficiencies of 25 and 40%, respectively.[34] For E_{hull}, previous successful high-throughput screening efforts[35] have shown that an upper threshold of 50 meV/atom yields materials that are reasonably synthesizable, and the experimentally known phosphor hosts in Table 1 have E_{hull} between 0 and 31 meV/atom. We will therefore adopt $E_{hull} < 50$ meV/atom as the stability threshold in this work.

Screening for New Narrow-Band Red-Emitting Phosphors. Figure 3 provides an overview of the high-throughput screening approach, which is tiered based on the relative computational expense to calculate the screening properties. An initial list of candidate structures was first generated from all existing ternary and quaternary nitrides in the Materials Project database,[18] which contains the precomputed data for all

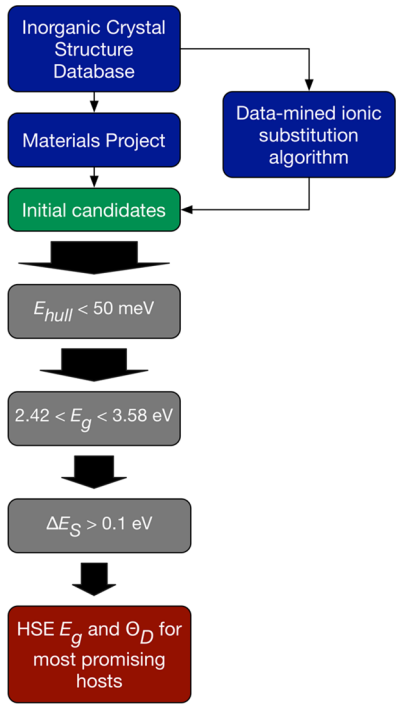

Figure 3. Flowchart showing high-throughput screening procedure for narrow-band red-emitting phosphor hosts. The relative size of the black arrows is an indicator of the number of materials remaining after each stage of screening.

ordered known inorganic crystals from the Inorganic Crystal Structure Database (ICSD). To augment this data set, a prediction of novel nitridosilicate and nitriodoaluminate structures with formula $A_xB_yC_zN_n$ (A = Ca/Sr/Ba, B = Li/Mg, C = Al/Si) was carried out by applying the data-mined ionic substitution algorithm proposed by Hautier et al.[36] on all crystal structures in the ICSD.[37] This focused structure prediction effort is motivated by the fact that nitridosilicate and nitriodoaluminate hosts have thus far demonstrated the greatest promise as narrow-band red emitters. In the first screening stage, all materials with $E_{hull} > 50$ meV, indicating that they are unlikely to be stable, were screened out. This was followed by further screening for candidates with 2.42 eV < PBE E_g < 3.58 eV. Finally, the 4f band levels of the Eu^{2+}-activated host were calculated to find narrow-band emitters with $\Delta E_S > 0.1$ eV. The HSE E_g and Θ_D were then computed for all materials that remain.

In total, 2259 (203 ternary, 156 quaternary, and 1900 predicted nitridosilicate and nitriodoaluminate quarternary structures) materials were evaluated for their phase stability (E_{hull}), emission wavelength, thermal quenching resistance (E_g and Θ_D), and emission bandwidth (ΔE_S). A total of eight narrow-band red-emitting phosphor hosts were identified from our high-throughput screening. Their calculated properties are summarized in Table 2, and their band structures (Figure S5) and crystal structures are provided in the Supporting Information. The calculated properties of 40 other hosts that satisfy all screening criteria with the exception of $\Delta E_S > 0.1$ eV, i.e., they are predicted to be broad-band red-emitting phosphors, are given in Table S1. Where there are multiple distinct sites for Eu^{2+} doping, the relative energies and phosphor properties based on Eu^{2+} activation on each distinct site are reported. Three of the identified materials, $CaLiAl_3N_4$

DOI: 10.1021/acs.chemmater.6b01496
Chem. Mater. 2016, 28, 4024−4031

Table 2. Calculated Properties of Eight Predicted Hosts and the Corresponding Eu^{2+}-Activated Phosphors[a]

materials	space group	E_{hull} (meV)	E_g (eV) PBE	E_g (eV) HSE	Θ_D (K)	E_{site} (meV/Eu)	ΔE_S (eV)
			New Phosphor Hosts				
$SrMg_3SiN_4$	$P\bar{1}$	2	2.49	3.66	634	0	0.124
						17	0.115
$SrLiAl_3N_4$	$I4_1/a$	3	2.93	4.12	716	0	0.139
$CaLiAl_3N_4$	$P\bar{1}$	14	3.00	4.28	742	0	0.132
						19	0.143
$BaLiAl_3N_4$	$P\bar{1}$	28	2.46	3.64	655	0	0.125
						61	0.101
$SrLiAl_3N_4$[b]	$P\bar{1}$	48	2.57	3.75	704	0	0.117
			Known Phosphor Hosts				
$SrLiAl_3N_4$[b]	$P\bar{1}$	0	2.97	4.47	716	0	0.139
						17	0.119
$SrMg_3SiN_4$	$I4_1/a$	0	2.42	3.68	648	0	0.119
$CaLiAl_3N_4$	$I4_1/a$	13	3.04	4.45	743	0	0.150

[a] E_{hull}, band gap E_g, Θ_D, relative site energy E_{site}, and narrow-band descriptor ΔE_S were calculated using the PBE functional with a Hubbard U of 2.5 eV for Eu. In addition, more accurate E_g values were calculated using the HSE functional. Materials are sorted by stability (E_{hull}). [b] Although these two materials have the same formula and space group, they are distinct crystal structures. See the Supporting Information.

($I4_1/a$), $SrLiAl_3N_4$ ($P\bar{1}$), and $SrMg_3SiN_4$ ($I4_1/a$), have already been previously reported experimentally as narrow-band red-emitting phosphors, which provides a good validation of our screening approach.

Five of the identified hosts are new materials that have not been previously reported as narrow-band red-emitting phosphors. All five new phosphor hosts belong to three structural prototypes. $CaLiAl_3N_4$ ($P\bar{1}$), $SrMg_3SiN_4$ ($P\bar{1}$), and $BaLiAl_3N_4$ ($P\bar{1}$) are isostructural with $CsNa_3TiO_4$ ($P\bar{1}$).[38] $SrLiAl_3N_4$ ($I4_1/a$) and $SrLiAl_3N_4$ ($P\bar{1}$) are isostructural with $NaLi_3SiO_4$ ($I4_1/a$)[39] and KLi_3PbO_4 ($P\bar{1}$),[40] respectively. $SrMg_3SiN_4$ ($P\bar{1}$), $SrLiAl_3N_4$ ($I4_1/a$), and $CaLiAl_3N_4$ ($P\bar{1}$) are particularly promising because they are predicted to have good phase stability (low E_{hull}), a highly rigid crystal structure (Θ_D > 600 K), a HSE band gap within the screening range, and a large splitting in the top two Eu^{2+} 4f bands (ΔE_S > 0.1 eV). $BaLiAl_3N_4$ ($P\bar{1}$) and $SrLiAl_3N_4$ ($P\bar{1}$) have somewhat higher E_{hull}, indicating that they may be more challenging to synthesize. Although $CaLiAl_3N_4$ and $SrMg_3SiN_4$ (all $P\bar{1}$) have multiple distinct Eu^{2+} activator sites, there is a clear energetic preference (>15 meV) for one of the sites, and all sites satisfy the criteria for narrow-band emission (ΔE_S > 0.1 eV). We have tested the sensitivity of the screening to changes in the ΔE_S threshold by plotting the ΔE_S of all known and predicted hosts studied in this work in Figure 4. We find that there is a distinct separation in the ΔE_S between broad-band (ΔE_S < 0.085 eV) and narrow-band emitters (ΔE_S > 0.1 eV). Therefore, small variations in the threshold do not affect the screening results significantly.

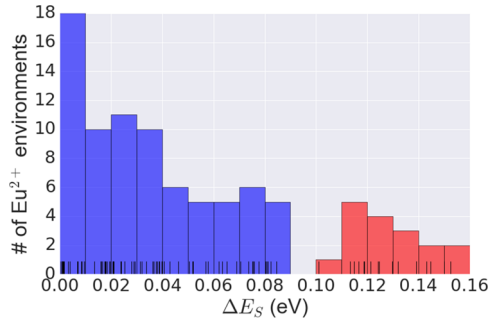

Figure 4. Distribution of computed narrow-band descriptor value ΔE_S for all distinct Eu^{2+} environments evaluated. Red bars indicate the number of environments that are above the 0.1 eV threshold, and blue bars indicate the number of environments below the 0.1 eV threshold. Black lines at the bottom of the plot indicate actual observed ΔE_S values. All known narrow- and broad-band phosphors fall into the red and blue regions, respectively.

DISCUSSION

Narrow-band red-emitting phosphors are a critical component for efficient, warm-light solid-state lighting. By combining a newly discovered electronic structure descriptor with an intelligently tiered high-throughput computational screening of known and predicted nitrides, we have identified five new narrow-band red-emitters that are predicted to exhibit good stability, red emission, narrow emission bandwidth, and good thermal quenching properties.

All new narrow-band red-emitting phosphor hosts identified in the high-throughput screening are predicted compounds from the data-mined ionic substitution algorithm. No existing nitrides in the Materials Project database were identified as promising hosts for narrow-band red emission. To gain further insight into the structural and chemical features that result in narrow-band emission, we have conducted in-depth analyses into the local environment and electronic structure of both the known and newly predicted narrow-band red-emitters.

We find that narrow-band emission is indicated only when the Eu^{2+} activator is in one of two highly unusual local environments: (i) an eight-coordinate cuboid-like environment, which is observed in most of the known and predicted narrow-band emitters, including the recently reported $SrLiAl_3N_4:Eu^{2+}$,[5] and (ii) a nine-coordinate environment, which has thus far been observed only in the narrow-band green emitter β-SiAlON:Eu^{2+}. On the other hand, no broad-band emitters (both known and predicted) exhibit these local environments. These observations suggest that these highly unusual Eu^{2+} environments are responsible for a crystal field splitting that results in a large gap between the two highest Eu^{2+} 4f bands. We have extracted the partial charge densities from the computed wave functions to determine the orientation of the charge

DOI: 10.1021/acs.chemmater.6b01496
Chem. Mater. 2016, 28, 4024−4031

distribution of the individual 4f bands relative to the N^{3-} ligands.

Figure 5 shows the partial charge density of the highest 4f band (at the Fermi level) in the Eu^{2+}-activated $CaLiAl_3N_4$ ($I4_1$/

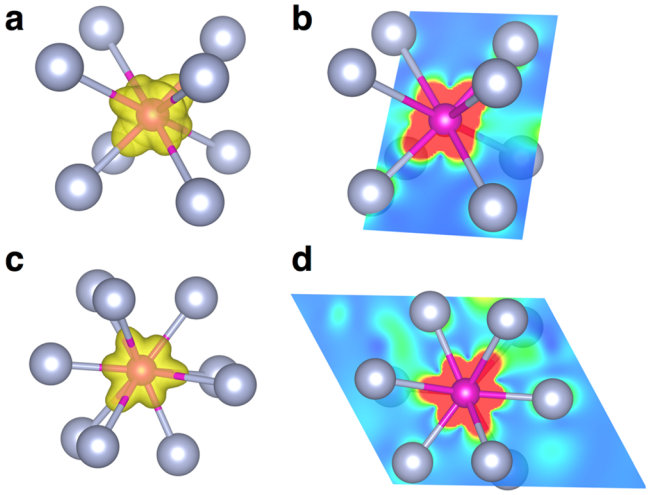

Figure 5. Partial charge density of the highest energy Eu^{2+} 4f band. (a, c) Isosurfaces at 0.0005 e/a_0^3 (a_0 is the Bohr radius) of the partial charge density of the highest energy Eu^{2+} 4f band (at the Fermi level) in $CaLiAl_3N_4$:Eu^{2+} (cuboid-like EuN_8 environment) and in β-SiAlON:Eu^{2+} (highly symmetrical EuN_9 environment), respectively. Maroon spheres, Eu; gray spheres, N. (b) Cross-section of the charge density passing through an Eu atom and approximately in the (110) diagonal plane of the cube in $CaLiAl_3N_4$:Eu^{2+}. (d) Cross-section of the charge density passing through an Eu atom and approximately in the (001) of the EuN_9 in β-SiAlON:Eu^{2+}.

a) and β-SiAlON phosphors. We have selected $CaLiAl_3N_4$:Eu^{2+} as a representative phosphor with the EuN_8 cuboid-like environment but have confirmed that the same features are observed in all phosphors with Eu^{2+} in a cuboid-like local environment. We find that the partial charge density for the highest 4f band of the EuN_8 environment exhibits a cuboid-like distribution, similar to the atomic $4f_{xyz}$ or $4f_{zx^2-zy^2}$ orbitals, directed along the Eu−N bonds. For the EuN_9 environment in β-SiAlON, the partial charge density exhibits a highly symmetric hexagonal distribution, similar to the atomic $4f_{x^3-3xy^2}$, $4f_{y^3-3yx^2}$, $4f_{5yz^2-yr^2}$, or $4f_{5xz^2-xr^2}$ orbitals, with three of the "lobes" aligned with an Eu−N bond each and the other three "lobes" approximately bisecting a pair of Eu−N bonds each. In contrast, no such alignment with Eu−N bonds is observed in the partial charge density of the lower 4f bands (Figures S6 and S7). From a crystal field perspective, a 4f band in either of these special alignments is penalized due to its proximity to the N^{3-} ligands, resulting in a significantly higher energy compared to that of the other 4f bands.

The implications of our findings go beyond the identification of the five new narrow-band red-emitting phosphors. Previous works have generally attributed narrow-band emission to restricted structural relaxation of the activator in its excited state due to the high symmetry of the cuboid environment.[5] Although we do not rule such constrained relaxation out as a contributing factor, our work suggests that the primary determinant of narrow-band emission is the effect of a highly symmetric crystal field on a highly localized, atomic-like Eu^{2+} 4f orbital, resulting in a large splitting in the top two bands, an effect that can be observed in the *ground-state* band structure. Thus far, only the highly unusual cuboid-like environment and nine-coordinated β-SiAlON environments are observed to have this effect. An open question is whether other coordination environments can be designed to induce a similar electronic structure feature for narrow-band emission in Eu^{2+} or other activators and will be the subject of further investigations.

Although the focus of our screening efforts in this work is on narrow-band red emitters, the high-throughput first-principles screening approach outlined can be readily extended to other emission wavelengths with a desired emission bandwidth. For instance, narrow-band green emitters are also required for ultraefficient solid-state lighting and LED-backlit LCD displays,[12,41] and we have demonstrated that the narrow-band descriptor is applicable to green emitters as well (Figure 1c). Conversely, broad-band emission is desired in certain applications to improve CRI, and by suitable inversion of the descriptor and tuning of the screening criteria, broad-band emitting phosphors at a desired wavelength may be identified.

Finally, we should note that there are certain limitations inherent in a high-throughput first-principles screening effort. For example, the Eu^{2+} activator concentration is known to affect the emission peak position,[28,34] an effect that is not captured in our screening. Also, only isovalent substitution of Eu^{2+} for other M^{2+} (e.g., Sr^{2+}, Ca^{2+}, and Ba^{2+}) is considered in the construction of the doped phosphor, and no attempt was made to find potential aliovalent substitutions that may generate other phosphor candidates. Ultimately, the proposed new hosts would need to be synthesized, verified, and further optimized experimentally. The fact that several of the proposed hosts are chemically similar to known phosphors gives us reasonable confidence that they are synthesizable.

CONCLUSIONS

In summary, we have demonstrated that an electronic structure characteristic in narrow-band Eu^{2+}-activated phosphors is a large splitting of >0.1 eV between the two highest Eu^{2+} 4f bands. By screening 2259 ternary, quaternary, and predicted nitride compounds on this descriptor and other calculated properties, we have identified five highly promising candidate hosts for Eu^{2+}-activated red-emitting phosphors that are predicted to exhibit chemical stability, good thermal quenching resistance and quantum efficiency, and narrow emission bandwidth. We have also shown evidence that narrow-band emission is the result of the crystal-field splitting of the Eu^{2+} 4f orbitals in a cuboid or highly symmetrical EuN_9 environment, which provides new insights into the emission characteristics of rare-earth dopants in phosphor hosts. The screening strategy in this work provides a general pathway to the discovery of new phosphors with a desired emission color and bandwidth for solid-state lighting.

ASSOCIATED CONTENT

Supporting Information

The Supporting Information is available free of charge on the ACS Publications website at DOI: 10.1021/acs.chemmater.6b01496.

Band structures and densities of states of known and new phosphors; U_{eff} effect on the narrow-band descriptor; relationship between ΔE_S and experimental fwhm; relationship between emission wavelength and PBE band gap; table of computed data of broad-band Eu^{2+}

DOI: 10.1021/acs.chemmater.6b01496
Chem. Mater. 2016, 28, 4024−4031

phosphor hosts; and partial charge density plots of lower 4f bands of $CaLiAl_3N_4:Eu^{2+}$ and β-SiAlON:Eu^{2+} (PDF) Crystallographic information files of predicted narrow-band red phosphors (ZIP)

AUTHOR INFORMATION

Corresponding Author

*E-mail: ongsp@eng.ucsd.edu.

Notes

The authors declare the following competing financial interest(s): Zhenbin Wang, Iek-Heng Chu, and Shyue Ping Ong have filed a provisional patent on the high-throughput screening methodology and new phosphors identified in this work.

ACKNOWLEDGMENTS

This work was supported by the National Science Foundation under grant no. 1411192. Some of the computations in this work were performed using the Extreme Science and Engineering Discovery Environment (XSEDE), which is supported by National Science Foundation grant no. ACI-1053575. Part of the work by Fei Zhou was performed under the auspices of the U.S. DOE by Lawrence Livermore National Laboratory under contract DE-AC52-07NA27344.

REFERENCES

(1) Uheda, K.; Hirosaki, N.; Yamamoto, Y.; Naito, A.; Nakajima, T.; Yamamoto, H. Luminescence Properties of a Red Phosphor, $CaAlSiN_3:Eu^{2+}$, for White Light-Emitting Diodes. *Electrochem. Solid-State Lett.* **2006**, *9*, H22.

(2) Piao, X.; Machida, K.; Horikawa, T.; Hanzawa, H.; Shimomura, Y.; Kijima, N. Preparation of $CaAlSiN_3:Eu^{2+}$ Phosphors by the Self-Propagating High-Temperature Synthesis and Their Luminescent Properties. *Chem. Mater.* **2007**, *19*, 4592−4599.

(3) Li, Y. Q.; Hirosaki, N.; Xie, R. J.; Takeda, T.; Mitomo, M. Yellow-Orange-Emitting $CaAlSiN_3:Ce^{3+}$ Phosphor: Structure, Photoluminescence, and Application in White LEDs. *Chem. Mater.* **2008**, *20*, 6704−6714.

(4) Zeuner, M.; Hintze, F.; Schnick, W. Low Temperature Precursor Route for Highly Efficient Spherically Shaped LED-Phosphors $M_2Si_5N_8:Eu^{2+}$ (M = Eu, Sr, Ba). *Chem. Mater.* **2009**, *21*, 336−342.

(5) Pust, P.; Weiler, V.; Hecht, C.; Tücks, A.; Wochnik, A. S.; Henß, A.-K.; Wiechert, D.; Scheu, C.; Schmidt, P. J.; Schnick, W. Narrow-Band Red-Emitting $Sr[LiAl_3N_4]:Eu^{2+}$ as a Next-Generation LED-Phosphor Material. *Nat. Mater.* **2014**, *13*, 891−896.

(6) Pust, P.; Wochnik, A. S.; Baumann, E.; Schmidt, P. J.; Wiechert, D.; Scheu, C.; Schnick, W. $Ca[LiAl_3N_4]:Eu^{2+}$—a Narrow-Band Red-Emitting Nitridolithoaluminate. *Chem. Mater.* **2014**, *26*, 3544−3549.

(7) Schmiechen, S.; Schneider, H.; Wagatha, P.; Hecht, C.; Schmidt, P. J.; Schnick, W. Toward New Phosphors for Application in Illumination-Grade White pc-LEDs: The Nitridomagnesosilicates $Ca[Mg_3SiN_4]:Ce^{3+}$, $Sr[Mg_3SiN_4]:Eu^{2+}$, and $Eu[Mg_3SiN_4]$. *Chem. Mater.* **2014**, *26*, 2712−2719.

(8) Xie, R.-J.; Hirosaki, N.; Li, Y.; Takeda, T. Rare-Earth Activated Nitride Phosphors: Synthesis, Luminescence and Applications. *Materials* **2010**, *3*, 3777−3793.

(9) Xie, R.-J.; Hirosaki, N.; Takeda, T.; Suehiro, T. On the Performance Enhancement of Nitride Phosphors as Spectral Conversion Materials in Solid State Lighting. *ECS J. Solid State Sci. Technol.* **2013**, *2*, R3031−R3040.

(10) Xie, R.-J.; Bert Hintzen, H. T. Optical Properties of (Oxy)nitride Materials: A Review. *J. Am. Ceram. Soc.* **2013**, *96*, 665−687.

(11) Bardsley, N.; Bland, S.; Pattison, L.; Pattison, M.; Stober, K.; Welsh, F.; Yamada, M. *Solid-State Lighting Research and Development Multi-Year Program Plan*; U.S. Department of Energy, 2014

(12) Phillips, J. M.; Coltrin, M. E.; Crawford, M. H.; Fischer, A. J.; Krames, M. R.; Mueller-Mach, R.; Mueller, G. O.; Ohno, Y.; Rohwer, L. E. S.; Simmons, J. A.; Tsao, J. Y. Research Challenges to Ultra-Efficient Inorganic Solid-State Lighting. *Laser Photonics Rev.* **2007**, *1*, 307−333.

(13) Kresse, G.; Furthmüller, J. Efficient Iterative Schemes for Ab Initio Total-Energy Calculations Using a Plane-Wave Basis Set. *Phys. Rev. B: Condens. Matter Mater. Phys.* **1996**, *54*, 11169−11186.

(14) Blöchl, P. E. Projector Augmented-Wave Method. *Phys. Rev. B: Condens. Matter Mater. Phys.* **1994**, *50*, 17953−17979.

(15) Perdew, J. P.; Burke, K.; Ernzerhof, M. Generalized Gradient Approximation Made Simple. *Phys. Rev. Lett.* **1997**, *78*, 1396−1396.

(16) Ong, S. P.; Richards, W. D.; Jain, A.; Hautier, G.; Kocher, M.; Cholia, S.; Gunter, D.; Chevrier, V. L.; Persson, K. A.; Ceder, G. Python Materials Genomics (Pymatgen): A Robust, Open-Source Python Library for Materials Analysis. *Comput. Mater. Sci.* **2013**, *68*, 314−319.

(17) Ong, S. P.; Wang, L.; Kang, B.; Ceder, G. Li−Fe−P−O_2 Phase Diagram from First Principles Calculations. *Chem. Mater.* **2008**, *20*, 1798−1807.

(18) Jain, A.; Ong, S. P.; Hautier, G.; Chen, W.; Richards, W. D.; Dacek, S.; Cholia, S.; Gunter, D.; Skinner, D.; Ceder, G.; Persson, K. A. Commentary: The Materials Project: A Materials Genome Approach to Accelerating Materials Innovation. *APL Mater.* **2013**, *1*, 011002.

(19) Ong, S. P.; Cholia, S.; Jain, A.; Brafman, M.; Gunter, D.; Ceder, G.; Persson, K. a. The Materials Application Programming Interface (API): A Simple, Flexible and Efficient API for Materials Data Based on REpresentational State Transfer (REST) Principles. *Comput. Mater. Sci.* **2015**, *97*, 209−215.

(20) Heyd, J.; Scuseria, G. E.; Ernzerhof, M. Hybrid Functionals Based on a Screened Coulomb Potential. *J. Chem. Phys.* **2003**, *118*, 8207.

(21) Heyd, J.; Scuseria, G. E.; Ernzerhof, M. Erratum: "Hybrid Functionals Based on a Screened Coulomb Potential. *J. Chem. Phys.* **2003**, *118*, 8207; *J. Chem. Phys.* **2006**, *124*, 219906.

(22) Dudarev, S. L.; Botton, G. A.; Savrasov, S. Y.; Humphreys, C. J.; Sutton, A. P. Electron-Energy-Loss Spectra and the Structural Stability of Nickel Oxide: An LSDA+U Study. *Phys. Rev. B: Condens. Matter Mater. Phys.* **1998**, *57*, 1505−1509.

(23) Chaudhry, A.; Boutchko, R.; Chourou, S.; Zhang, G.; Grønbech-Jensen, N.; Canning, A. First-Principles Study of Luminescence in Eu^{2+}-Doped Inorganic Scintillators. *Phys. Rev. B: Condens. Matter Mater. Phys.* **2014**, *89*, 155105.

(24) Brgoch, J.; DenBaars, S. P.; Seshadri, R. Proxies from Ab Initio Calculations for Screening Efficient Ce^{3+} Phosphor Hosts. *J. Phys. Chem. C* **2013**, *117*, 17955−17959.

(25) Hill, R. The Elastic Behaviour of a Crystalline Aggregate. *Proc. Phys. Soc., London, Sect. A* **1952**, *65*, 349−354.

(26) Strobel, P.; Schmiechen, S.; Siegert, M.; Tücks, A.; Schmidt, P. J.; Schnick, W. Narrow-Band Green Emitting Nitridolithoalumosilicate $Ba[Li_2(Al_2Si_2)N_6]:Eu^{2+}$ with Framework Topology Whj for LED/LCD-Backlighting Applications. *Chem. Mater.* **2015**, *27*, 6109−6115.

(27) Hirosaki, N.; Xie, R.-J.; Kimoto, K.; Sekiguchi, T.; Yamamoto, Y.; Suehiro, T.; Mitomo, M. Characterization and Properties of Green-Emitting β-SiAlON:Eu^{2+} Powder Phosphors for White Light-Emitting Diodes. *Appl. Phys. Lett.* **2005**, *86*, 211905.

(28) Li, Y. Q.; van Steen, J. E. J.; van Krevel, J. W. H.; Botty, G.; Delsing, A. C. A.; DiSalvo, F. J.; de With, G.; Hintzen, H. T. Luminescence Properties of Red-Emitting $M_2Si_5N_8:Eu^{2+}$ (M = Ca, Sr, Ba) LED Conversion Phosphors. *J. Alloys Compd.* **2006**, *417*, 273−279.

(29) Hecht, C.; Stadler, F.; Schmidt, P. J.; auf der Günne, J. S.; Baumann, V.; Schnick, W. $SrAlSi_4N_7:Eu^{2+}$—a Nitridoalumosilicate Phosphor for Warm White Light (pc)LEDs with Edge-Sharing Tetrahedra. *Chem. Mater.* **2009**, *21*, 1595−1601.

(30) Dorenbos, P. Thermal Quenching of Eu^{2+} 5d−4f Luminescence in Inorganic Compounds. *J. Phys.: Condens. Matter* **2005**, *17*, 8103−8111.

DOI: 10.1021/acs.chemmater.6b01496
Chem. Mater. 2016, 28, 4024−4031

(31) Cohen, A. J.; Mori-Sanchez, P.; Yang, W. Insights into Current Limitations of Density Functional Theory. *Science* **2008**, *321*, 792−794.
(32) Setyawan, W.; Gaume, R. M.; Lam, S.; Feigelson, R. S.; Curtarolo, S. High-Throughput Combinatorial Database of Electronic Band Structures for Inorganic Scintillator Materials. *ACS Comb. Sci.* **2011**, *13*, 382−390.
(33) Gál, Z. A.; Mallinson, P. M.; Orchard, H. J.; Clarke, S. J. Synthesis and Structure of Alkaline Earth Silicon Nitrides: $BaSiN_2$, $SrSiN_2$, and $CaSiN_2$. *Inorg. Chem.* **2004**, *43*, 3998−4006.
(34) Duan, C. J.; Wang, X. J.; Otten, W. M.; Delsing, A. C. A.; Zhao, J. T.; Hintzen, H. T. Preparation, Electronic Structure, and Photoluminescence Properties of Eu^{2+}- and Ce^{3+}/Li^{+} -Activated Alkaline Earth Silicon Nitride $MSiN_2$ (M = Sr, Ba). *Chem. Mater.* **2008**, *20*, 1597−1605.
(35) Hautier, G.; Jain, A.; Ong, S. P.; Kang, B.; Moore, C.; Doe, R.; Ceder, G. Phosphates as Lithium-Ion Battery Cathodes: An Evaluation Based on High-Throughput Ab Initio Calculations. *Chem. Mater.* **2011**, *23*, 3495−3508.
(36) Hautier, G.; Fischer, C.; Ehrlacher, V.; Jain, A.; Ceder, G. Data Mined Ionic Substitutions for the Discovery of New Compounds. *Inorg. Chem.* **2011**, *50*, 656−663.
(37) Bergerhoff, G.; Hundt, R.; Sievers, R.; Brown, I. D. The Inorganic Crystal Structure Data Base. *J. Chem. Inf. Model.* **1983**, *23*, 66−69.
(38) Weiß, C.; Hoppe, R. The New Orthotitanate $CsNa_3[TiO_4][1]$. *Z. Anorg. Allg. Chem.* **1996**, *622*, 1715−1720.
(39) Nowitzki, B.; Hoppe, R. Neues Uber Oxide Vom Typ $A[(TO)_n]$: $NaLi_3SiO_4$, $NaLi_3GeO_4$ Und $NaLi_3TiO_4$. *Rev. Chim. Min.* **1986**, *23*, 217−230.
(40) Brazel, V. B.; Hoppe, R. Fragmentierung" und "Aggregation" bei Bleioxiden. Ueber Das Oligooxoplumbat(IV) $K_2Li_6(Pb_2O_8)$. *Z. Anorg. Allg. Chem.* **1983**, *497*, 176−184.
(41) Wang, L.; Wang, X.; Kohsei, T.; Yoshimura, K.-I.; Izumi, M.; Hirosaki, N.; Xie, R.-J. Highly Efficient Narrow-Band Green and Red Phosphors Enabling Wider Color-Gamut LED Backlight for More Brilliant Displays. *Opt. Express* **2015**, *23*, 28707−28717.
(42) Tolhurst, T. M.; Boyko, T. D.; Pust, P.; Johnson, N. W.; Schnick, W.; Moewes, A. Investigations of the Electronic Structure and Bandgap of the Next-Generation LED-Phosphor $Sr[LiAl_3N_4]:Eu^{2+}$-Experiment and Calculations. *Adv. Opt. Mater.* **2015**, *3*, 546−550.
(43) Fang, C. M.; Hintzen, H. T.; With, G. de; Groot, R. A. de. Electronic Structure of the Alkaline-Earth Silicon Nitrides $M_2Si_5N_8$ (M = Ca and Sr) Obtained from First-Principles Calculations and Optical Reflectance Spectra. *J. Phys.: Condens. Matter* **2001**, *13*, 67−76.

DOI: 10.1021/acs.chemmater.6b01496
Chem. Mater. 2016, 28, 4024−4031